Journal of Alloys and Compounds 791 (2019) 109–120

Contents lists available at ScienceDirect

Journal of Alloys and Compounds

journal homepage: http://www.elsevier.com/locate/jalcom

Mechanistic understanding, gamma phase formation and morphological behaviour of the Reduction–Diffusion processed U-Mo alloy

Sonal Gupta [a,*], Raj Kumar [a], Sanjib Majumdar [b], Jitendra Sonber [b], S.K. Satpati [a], M.L. Sahu [a]

[a] *Uranium Extraction Division, Bhabha Atomic Research Centre, Mumbai 400085, India*
[b] *Materials Processing & Corrosion Engineering Division, Bhabha Atomic Research Centre, Mumbai 400085, India*

ARTICLE INFO

Article history:
Received 3 December 2018
Received in revised form
15 February 2019
Accepted 13 March 2019
Available online 16 March 2019

Keywords:
Actinide alloys and compounds
Nuclear reactor materials
Powder metallurgy
Diffusion
Scanning electron microscopy
SEM
X-ray diffraction

ABSTRACT

Reduction–Diffusion (R-D) process has been attempted to synthesize U-Mo alloy powder for the first time, and the mechanism of alloy formation has been investigated. Calciothermic reduction of uranium dioxide in the presence of the alloying element Mo, followed by high temperature soaking; subsequent leaching to remove the calcia slag yields U-Mo alloy in powder form. Experiments were carried out to synthesize U-10 wt%Mo alloy powder. The alloy powder products were characterized by Scanning Electron Microscopy and X-ray Diffraction. Complete stabilization of the metastable isotropic gamma phase has been achieved in U-10 wt%Mo powder synthesized by R-D process, where the final soaking was carried out at 1300 °C and 4 h. Attempts were made to understand the mechanism of formation of U-Mo alloy by R-D process on two fronts, i.e. alloying within a single particle, and particle-to-particle homogenization. The intended application of the alloy powders is in high uranium density dispersion fuels for high flux nuclear research and test reactors.

1. Introduction

High uranium density alloys and compounds are required for use in dispersion fuels, for high flux research and test reactors [1–5]. UAl_3, U_3Si, U_3Si_2, U_6Me (Me = Fe, Ni, Mn, Co or Ge), U–10 wt%Mo are some of the candidate alloys/compounds which have been studied in this regard [6–10]. Among them U-Mo alloys were found to be the most promising [3–5,11,12]. Unalloyed uranium has orthorhombic crystal structure from room temperature up to 663 °C (i.e. α-uranium) and hence is anisotropic and lacks dimensional stability and irradiation stability [3–5,13,14]. Alpha uranium transforms to beta uranium at 663 °C, which has tetragonal structure; beta uranium transforms to gamma uranium at 770 °C which is body – centred cubic [13]. The high temperature phase γ-uranium has body centred cubic crystal structure and hence it is isotropic and stable under irradiation environments, but not thermodynamically stable at room temperature. The γ-U is known to behave in a stable manner under low-burnup, high-temperature conditions, on account of swelling through fission gas nucleation and growth [4,5], unlike α-U which undergoes cavitational swelling under irradiation, and thermal and irradiation growth under power ramping [3,4]. In addition, γ-phase is desirable because of its resistance to corrosion in water and water – steam environments [11]. Hence, uranium needs to be alloyed with elements like Nb, Hf, Zr, Mo, Ti, Pu, Ru, Rh, Pd, Re which can stabilize the γ-phase for an indefinitely long period at room temperature, and for a long time period at elevated temperatures [3–5]. Among these, U-Mo alloys form γ-phase at relatively higher range of solute concentration, which makes them more favourable [15]. Alloying with Mo improves thermal cycling stability of uranium and also imparts superior fabrication characteristics [16]. Unalloyed alpha uranium is very brittle, whereas unalloyed gamma uranium is too soft and weak. The uranium density in the fuel cladded in Al matrix which is achieved with U-10 wt% Mo alloy is 8–9 g cm^{-3}, as compared to U_3Si_2 and UAl_3, where the densities are about 4.8 g cm^{-3} and 1.7–2.3 g cm^{-3} respectively [17,18]. In U-Mo alloys, the cubic γ-phase can be retained at room temperature by adding minimum 8 wt% Mo under furnace cooling condition, and by addition of

---

[*] Corresponding author.
E-mail address: sonalg@barc.gov.in (S. Gupta).

https://doi.org/10.1016/j.jallcom.2019.03.204
0925-8388/

4.2 wt% under critical cooling conditions [4,19]. However, for desired fuel behaviour and performance in the reactor, the retention of this metastable γ-phase in alloys at temperatures below 560 °C during fuel fabrication and irradiation is desirable, as the equilibrium phases in this temperature regime are orthorhombic α and tetragonal γ′ (U_2Mo) [3,5,20]. Literature studies report that with increased addition of Mo in U, the transformation becomes more and more "sluggish" [5,20]. Thus, U-10 wt% Mo is inherently stable against decomposition; hence the alloy of this composition has been the subject of interest of so many researchers, particularly after 1970s [1–5].

For use in the dispersion type fuels, U-Mo alloy is required in powder form. U-Mo alloy powder was prepared in the past by centrifugal atomization, rotating electrode process, hydriding-dehydriding (HDH) and mechanical grinding [12,18,21–26]. All these processes mentioned above require the starting material of U-Mo alloy ingot to be prepared by melting-casting and afterwards be subjected to the respective powder preparation technique.

Reduction-Diffusion (R-D) process is a novel method, which has been used predominantly for the synthesis of rare earth magnetic alloy powders directly from their oxides (or chlorides) [27,28]. The rare earth oxide (or chloride) is reduced using a suitable reductant, mostly calcium in the presence of the alloying element [27,28]. The reduced metal then forms alloy with the other metal in the charge by mutual diffusion, and the heat balance of the reaction is such that the alloy is directly obtained in powder form [27–29]. The alloy powder particles remain separated by solid calcium oxide slag network; hence on solidification and leaching to remove the slag, the final alloy is obtained in powder form [29]. R-D process has been a great success for the synthesis of Sm-Co, Nd-Fe-B, La-Ni, Sm-Fe, La-Fe-Si, Al-Ti, V-Ti, Y-Ni alloy powders [27,28,30–39]. However, no such work on the synthesis of U-Mo powder by R-D has been reported till date. The process is simpler and eliminates the need of melting the metals to form alloy ingot, and hence can be more cost-efficient process. In the present study, this method has been employed for the first time to prepare U-Mo alloy powder. A systematic comparison of the pros and cons of the various methods mentioned above along with the R-D method, is presented in Table 1.

The present study involves the preparation of U-Mo alloy powder by the calciothermic reduction (CTR) of uranium dioxide in the presence of Mo powder in the required stoichiometric amount at different times and temperatures, and characterization of the alloy powders using XRD and SEM. The residual calcium content was also analyzed for one of the representative powder samples using volumetric analysis methods. Attempts were made to understand the mechanism of alloying within a single particle and inter-particle homogenization mechanism, in R-D process in the U-Mo system.

2. Materials and methods

The R-D experiments were carried out in batches on a 100 g UO_2 scale. U-10 wt%Mo was the target alloy composition. Uranium dioxide of nuclear purity (>99.6% U) was prepared by the reduction of UO_3 with ammonia. UO_3 was obtained by calcining ammonium diuranate at 475 °C. Molybdenum metal powder (produced by hydrogen reduction of MoO_3) of 99.9% purity was used. Molybdenum powder was taken in 10% excess over the stoichiometric requirement for U-10 wt%Mo alloy, to ensure complete alloying and to account for volatilization of Mo as MoO_3. The raw materials were mixed in a double cone blender. The blended mixture was charged into a yttria-coated graphite crucible, and the remaining space of the crucible was capped with pre-calcined CaO. The crucible was then put inside a recrystallized alumina retort which had four connections; for thermocouple (B-type, Pt-Rh-30%/Pt-Rh-6%), argon inlet, argon outlet and vacuum. The retort was then loaded into a resistive pit-type furnace. The chamber was evacuated and back flushed with argon three times and thereafter argon was purged continuously to maintain an inert atmosphere. The heating schedule for the experiment was decided based on the observations of the DTA experiment (discussed in Results). DTA was carried out using *Setsys Evolution TGA-DTA/DSC* (Make: Setaram) to determine the onset of the reduction temperature. The final soaking temperatures and duration are indicated in Table 2. Soaking was done for alloying and homogenization. The reduced mass obtained after CTR was subjected to leaching with acetic acid in an agitated glass beaker. This was followed by washing with acetone and vacuum drying, whereby it finally turned into a silvery grey U alloy powder, followed by packing and sealing. Drying, packing and sealing were carried out under inert (argon) atmosphere inside glove box as U (metal/alloy) powder is pyrophoric. The presence of even a very small amount of air/oxygen can cause violent reaction of U and oxygen causing the powder to catch fire.

The alloy powder was characterized by X-Ray Diffraction and Scanning Electron Microscopy techniques. X-Ray diffraction was carried out using *INEL Equinox 3000 X-Ray Diffractometer* with curved Position Sensitive Detector with 2θ range from 0 to 120° and copper target with K-α of wavelength 1.54056 Å. The XRD acquisition was carried out for about 1 h (generator: 40 kV, 30 mA) to ensure that peaks corresponding to different phases develop with intensities good enough for analysis and get well resolved from the background (i.e. peak to background ratio should be high). PDF-2 is the reference database used for analysis using Match! Software®.

Table 1
Comparison of the different methods of alloy powder synthesis.

	Atomization/Rotating Electrode Process	Hydriding- Dehyriding (HDH) process	Reduction - Diffusion process
Pros	Tighter control over particle size distribution [40]	Does not require re-melting of ingot as in atomization, the solid ingot can be reacted with hydrogen directly and then de-hydrided.	• Simpler process, eliminates the need of melting the metals to form alloy ingot, process steps are reduced. • Raw material is oxide, does not require high purity metal as starting material
Cons	• Process steps are more • Alloy needs to be synthesized by melting-casting and is then re-melted for carrying out atomization (energy-intensive).	• Alloy ingot prepared by melting-casting which is then hydrided. • Gamma U-Mo hydride is not very brittle; hence milling operation needs to be carried out before dehydriding [26]. • HDH might be easy for U powder (brittle α-U hydride); but for alloy powder, process steps are more. • Very fine powders produced, which are difficult to handle and often pyrophoric	• Interaction between material of construction and alloy. However, in the present study this problem was overcome by using graphite crucible with yttria coating on it.

Table 2
Details of the process parameters of the different R-D experiments.

Exp. Code	Process Parameters	Sample Preparation for SEM
RD-1	1150 °C, 4 h	Powder sprinkled on graphite tape
RD-2	1300 °C, 1 h	Powder sprinkled on graphite tape, powder also mounted in cold setting resin and polished to reveal the cross-section
RD-3	1300 °C, 4 h	Powder sprinkled on graphite tape
RD-4	1300 °C, 5 min	Powder sprinkled on graphite tape, powder also mounted in cold setting resin and polished to reveal the cross-section
RD-5	970 °C, 4 h	Samples of reduced mass mounted in cold setting resin and polished to view the slag morphology

SEM and EDS were carried out using *CamScan Scanning Electron Microscope (Model: CamScan MV 100)* with tungsten filament and Energy Dispersive Spectrometer attachment of *Oxford Instruments (X-max 80)*. The accelerating voltage in the SEM was 20 kV.

The detailed chemical analysis of alloy powder of a representative batch was carried out to determine U, Mo, residual Ca, C, N and O concentrations. 1 g of the powder sample was dissolved in 2 N HNO_3 and titrated by potassium dichromate to get uranium concentration. To analyze Mo concentration, about 0.5 g of the powder sample was dissolved in 4 N HNO_3 and diluted to a make-up volume 25 mL. U was extracted from the solution by 30% TBP (Tri-Butyl Phosphate), it forms a complex with TBP. The solution free from U was analyzed by Inductively Coupled Plasma Atomic Emission Spectroscopy for Mo concentration. The same procedure was followed for residual Ca analysis. U has to be first removed from the solution because it exhibits various oxidation states, and hence has characteristic peaks in the entire region of the emission spectrum; which might interfere with the peaks of Ca and Mo.

To analyze nitrogen content, the sample was put inside a nickel flask and fused in a graphite crucible in purified helium atmosphere at 2700 °C. The released nitrogen as N_2 was passed through chemical traps and quantified from the thermal conductivity difference of reference gas flow (He) and sample gas flow (N_2 + He). The combustion of the alloy sample in purified oxygen atmosphere at ~1100 °C inside an induction furnace was carried out to detect carbon content; whereby carbon in the sample converted to CO_2. CO_2 was passed through chemical traps and amount of C is quantified by measuring the transmittance against the characteristic IR absorption peak of CO_2 at wave number 2350 cm^{-1} by employing IR detector. To determine oxygen content, the sample was put in nickel flask and fused in graphite crucible in purified helium atmosphere at 2700 °C. Oxygen is released as CO and traces of CO_2. All CO is oxidised to CO_2 by CuO. Oxygen is determined by quantification of CO_2 by IR detector.

3. Results

3.1. Thermal analysis

Differential thermal analysis was carried out to determine the temperature at which reduction of UO_2 by Ca takes place. The DTA plot is shown in Fig. 1. An endothermic peak at around 640 °C is observed, where weight loss is seen in the TG curve, which indicates volatilization of Mo as MoO_3 [41]. Two more endothermic peaks are observed, one between 830 and 840 °C and the other at ~1130 °C; which correspond to the melting of calcium and uranium, respectively. The melting points of Ca and U are 842 °C and 1132 °C respectively. An exothermic peak appears at around 850–900 °C, next to the melting of Ca which marks the onset of reduction of UO_2 to U metal. Melting of Ca triggers the reduction reaction by forming a uniform layer over the uranium oxide particles facilitating the reduction. There is a slight drop in the weight of the charge in the reduction region, which occurs due to local volatilization of Ca because of the heat released during reduction of UO_2. The initial drop in weight in the TG curve is due to the removal of moisture and volatile impurities during heating.

The heat of reduction reaction is sufficient to melt the uranium, but not sufficient to maintain U in molten state for prolonged time,

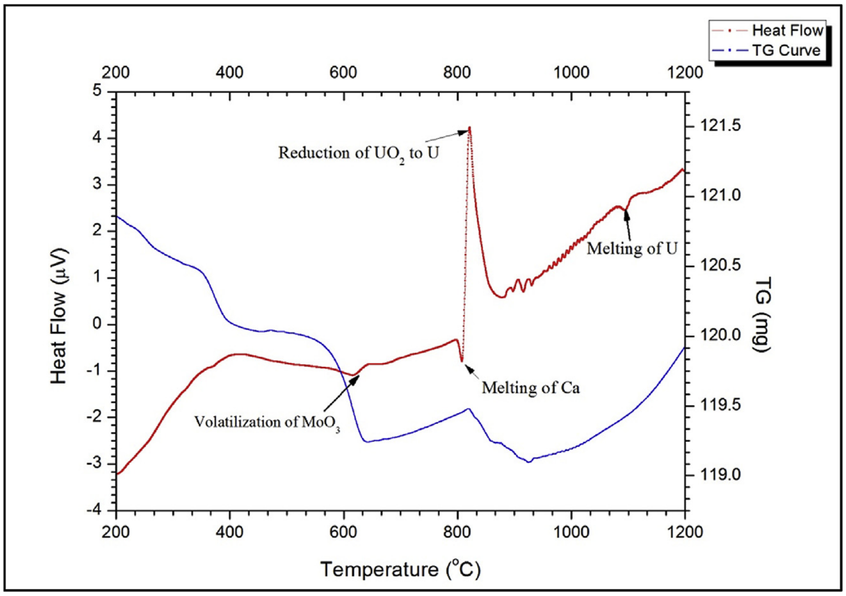

Fig. 1. The DTA-TG plot for calciothermic reduction of UO_2 in the presence of Mo.

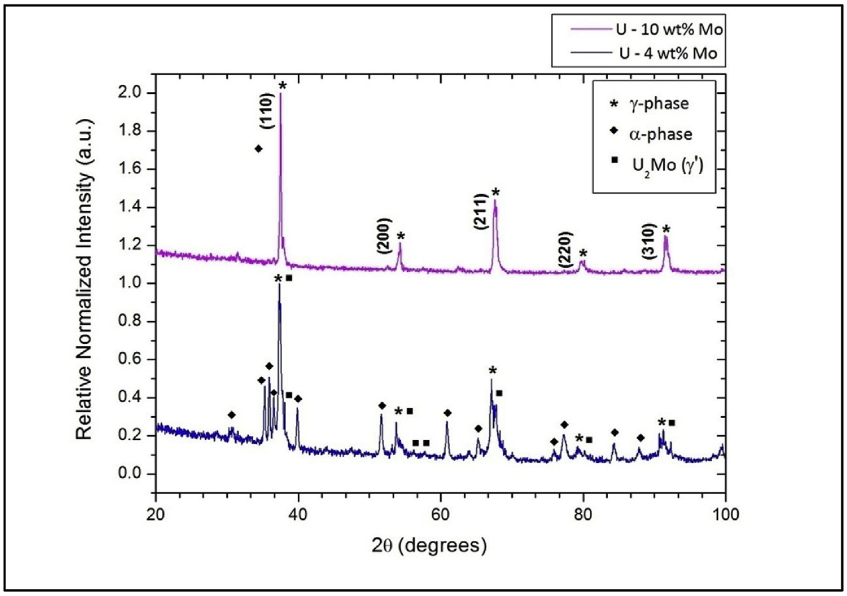

Fig. 2. The XRD plot of U-Mo alloy powders prepared by R-D process.

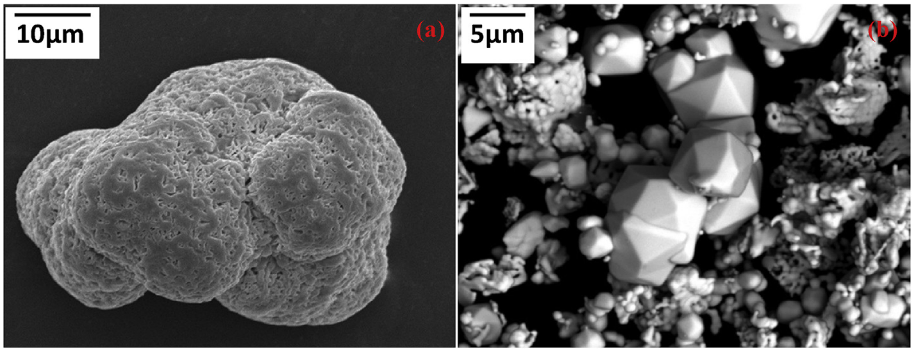

Fig. 3. SEM images of the raw materials used for the experiments, (a) UO_2 powder (b) Mo powder.

hence external heating is continued up to the final soaking temperature. To ensure efficient and complete reduction of oxide to U metal before melting of U occurs, it was decided to give a soaking of about 10 min at 900 °C in the main experimental trials.

3.2. Phase analysis

The XRD pattern shown in Fig. 2 is characteristic of the U-Mo alloy powders prepared by R-D process. The XRD plot of U-10 wt% Mo alloy which was soaked at 1300 °C for 4 h contains peaks corresponding to only γ-phase. Peaks corresponding to UO_2 (starting material) are not seen in the XRD plot. Both α and γ′ peaks are absent, which indicates complete stabilization of γ-phase under the mentioned soaking conditions. The XRD plot for one such experiment carried out with 4 wt% Mo under the same soaking conditions, showed the presence of all the three (α, γ′ and γ) phases, i.e. γ-phase was only partially stabilized. γ′ peaks occur at 2θ values which are very close to those corresponding to γ peaks; it is because γ' (tetragonal) is an ordered structure of the metastable γ (cubic) phase. Hence, it is difficult to distinguish between γ and γ′ peaks.

The entries in the PDF-2 database used to identify the phases in Match! Software® are 00-024-0748 (α-uranium), 00-024-0749 (γ-uranium) and 00-012-0296 (γ′ or U_2Mo).

3.3. Morphological and chemical analyses

3.3.1. Morphology

SEM images of the raw materials are shown in Fig. 3. It is clear that UO_2 particle (Fig. 3(a)) is porous and irregular in nature, and particles have size in the range of 20–30 μm. Mo powder particles exhibit two morphologies. Mo particles (Fig. 3(b)) of around ~10–15 μm are faceted. Except for these particles, most of the Mo powder particles are in the form of agglomerates of small faceted particles (individual particles of ~1 μm).

The effect of soaking temperature and soaking time on the final morphology and distribution of Mo in an alloy particle is illustrated in Fig. 4. In case of RD-3 (1300 °C, 4 h), the alloy particles exhibit two morphologies, one of rounded type and the other of skeleton-like structure (see Fig. 4(c)). The composition at the particle surface is close to 10 wt% Mo (as is evident from EDS point scan data, Fig. 4(h)) and the average composition obtained through the EDS

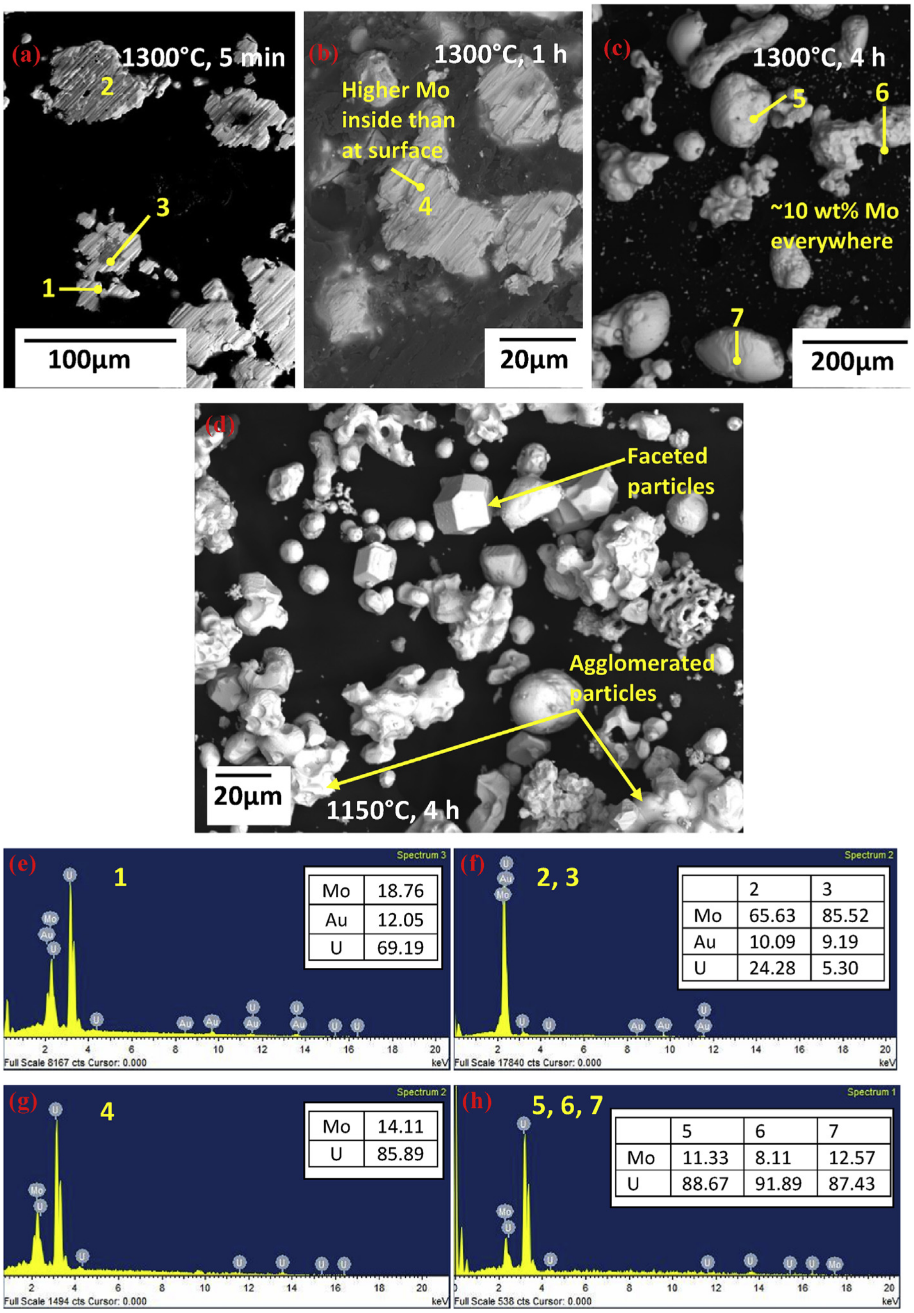

	1
Mo	18.76
Au	12.05
U	69.19

	2	3
Mo	65.63	85.52
Au	10.09	9.19
U	24.28	5.30

	4
Mo	14.11
U	85.89

	5	6	7
Mo	11.33	8.11	12.57
U	88.67	91.89	87.43

Fig. 4. SEM – BSE images of U-Mo alloy powders prepared by R-D process under different soaking conditions: (a) 1300 °C, 5 min (b) 1300 °C, 1 h (c) 1300 °C, 4 h (d) 1150 °C, 4 h; the corresponding EDS data for the points marked 1 through 7 are shown in the EDS spectrums Fig. 4(e)–4(h).

data is 10.58 wt% Mo. The Mo composition observed in the volumetric (bulk) analysis is also 9.7 wt% (Table 3). Thus, the Mo composition throughout the particle is about 10 wt%, which is also the Mo composition in every alloy particle.

When the soaking time was limited to 1 h at 1300 °C (RD-2), it was found that there was a large variation in the surface composition of the alloy particles (in EDS point scan), and apparently, some particles did not contain Mo at all. Hence, the particle was mounted and polished to reveal a particle cross-section, and the average Mo concentration analyzed over different points at the particle cross-section was found to be around 14 wt% (refer Fig. 4(b) and (g) for the SEM and corresponding EDS data respectively), which was higher than the Mo concentration at the surface, indicating that a Mo concentration gradient existed from particle core

Table 3
Chemical Analysis of the U-Mo alloy produced by the optimized R-D process.

Exp. Code	U wt%	Mo wt%	Ca wt%	O wt%	C wt%	N wt%
RD-3, U-10 wt% Mo	90.6 ± 0.3	9.7 ± 0.2	0.0445 ± 0.0022	0.0595 ± 0.0060	0.0195 ± 0.0020	0.0350 ± 0.0030

to surface, which if given sufficient soaking time, would have vanished due to homogenization. This was an important inference from RD-2, which provided an impetus for investigation of the alloying mechanism within a single particle. An experiment (RD-4) was planned to capture and analyze particles where incomplete alloying could be seen by soaking for just 5 min. As expected, unalloyed Mo was present in the core of the particle as seen in the SEM image in the backscattered mode (Fig. 4(a)). Hence, Mo concentration in the centre of the particle was close to 100%. The EDS results (refer Fig. 4(f)) quote this concentration as 85 wt% Mo (marked 3 in Fig. 4(a)), because part of the intensity (~9–10 wt%) is also attributed to gold, which was present because the mounted sample was coated with gold to make it conducting. The actual Mo concentration hence will be much greater than 85 wt% at the centre. The elemental maps for U and Mo distribution were obtained using EDS for the same alloy particle, as shown in Fig. 5. The system indicates a shrinking core type mechanism of alloy formation [42], which has been discussed in detail in Section 4.

The SEM image of RD-1 alloy which was soaked at 1150 °C (Fig. 4(d)) shows faceted morphology and also agglomerates of faceted particles, which resemble the morphology of the Mo powder used for the experiments. These particles of RD-1 powder confirm the presence of both U and Mo. Hence, it seems that the liquid U envelops the Mo particle, and dissolution of Mo into the U envelope increases the melting point of the U in the envelope, which therefore might have solidified under the temperature conditions of the system; hence the morphology of Mo powder is retained in the alloy powder particles.

The SEM images in Fig. 4 also depict that the particle size of the alloy powder is a function of soaking temperature and soaking time. However, to quantitatively correlate the particle size with the process parameters, further studies need to be done.

The reduced hard mass obtained after calciothermic reduction of UO_2 in RD-5 (970 °C, 4 h) was mounted and polished, and viewed under SEM to examine the morphology of the CaO slag which formed during the reduction reaction. The SEM images are shown in Fig. 6.

The temperature was chosen just above the temperature where reduction occurs. In general, every SEM image had three colours, white for the U alloy region, greyish to dark greyish for the CaO slag, and black for the empty pockets based upon Z contrast in back scattered electron imaging in SEM; and was confirmed by the EDS which was done for the same images (refer Fig. 6(e) and (f)). The U particles are in general spherical or rounded and are dispersed in the calcium oxide slag as is evident from Fig. 6(a) and (b). The CaO slag contains empty pockets or pores (see Fig. 6(b)), of irregular geometry, which are interconnected. Some interconnected particles which show signs of coalescence were also observed, as in Fig. 6(c) and (d). Presence of Au in the spectrum is due to the gold coating done to make the sample conducting, since it contains ceramic CaO slag.

3.3.2. Chemical composition

The sample which, through XRD and SEM/EDS analysis confirmed to be homogeneous U - 10 wt% Mo (RD-3) alloy powder was also analyzed for U wt%, Mo wt%, residual Ca and other impurities by the methods described in Section 2. The chemical composition of the respective sample is reported in Table 3.

4. Discussion

4.1. Mechanism and evolution of morphology

The reaction $UO_2 + 2Ca \rightarrow U + 2CaO$ is exothermic in nature ($\Delta H^{\circ}_{298} = -44.2$ kcal/mol, $\Delta G^{\circ}_{298} = -42.15$ kcal/mol, taken from *JANAF Tables*). As Mo dissolves in liquid uranium, the liquidus temperature of the alloy increases [43]. The liquidus of the concerned alloy U-10 wt%Mo is 1252 °C (see U-Mo phase diagram, Fig. 11, [43]). To understand the effect of temperature on the process, two temperatures were chosen, one above the alloy liquidus, i.e. 1300 °C and one between the melting point of U and the alloy, i.e. 1150 °C. Soaking above the alloy liquidus provides superheat to ensure that the alloy is molten and has sufficient flowability so that it can move through the pores of the CaO slag. The porous nature of CaO slag has been discussed in Section 3.3.1. The average composition of the alloy powder obtained under different soaking conditions and the standard deviation values calculated from the EDS data are reported in Table 4, which clearly indicate that the spread in the Mo concentration, i.e. the inhomogeneity decreases as the soaking time at higher temperature (1300 °C) increases. The spread in the Mo concentration is maximum ($\sigma = 25.57$) even with a soaking of 4 h when the soaking temperature is 1150 °C. This inhomogeneity is lower even for process parameters (1300 °C, 5 min) and (1300 °C, 1 h). Thus, it can be inferred that the soaking temperature must be well above the alloy liquidus; and at such a temperature, increasing the soaking time increases both the intra-particle homogeneity (i.e. absence of unalloyed Mo core inside the particle) and inter-particle homogeneity of the alloy powder.

4.1.1. Alloying within a single particle: the single-particle system

In experiment RD-4 (1300 °C, 5 min), large inhomogeneity is observed in the final alloy powder due to insufficient soaking time available. The powder was mounted and polished to reveal a cross-section of the particle, and then viewed under SEM in backscattered mode. The SEM (BSE) image shown in Fig. 4(a), shows dark grey patches on the white surface of the particle cross-section, which confirm the presence of Mo (low Z element, Z = 42) in EDS. The white region confirms the presence of U (high Z, Z = 92) with much smaller concentration of Mo than that in the core of the particle. The elemental map for U (in red colour) generated using EDS

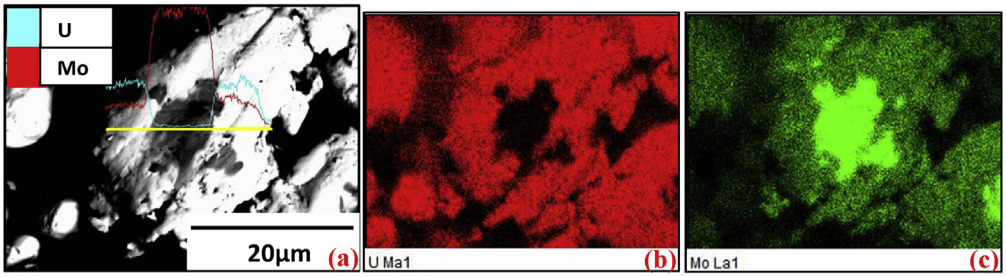

Fig. 5. (a) SEM – BSE image of the cross-section of an alloy particle which was soaked for 5 min at 1300 °C, line scan for U and Mo distribution through the cross-section is also shown (b) Elemental map for U distribution over the cross-section (c) Elemental map for Mo distribution.

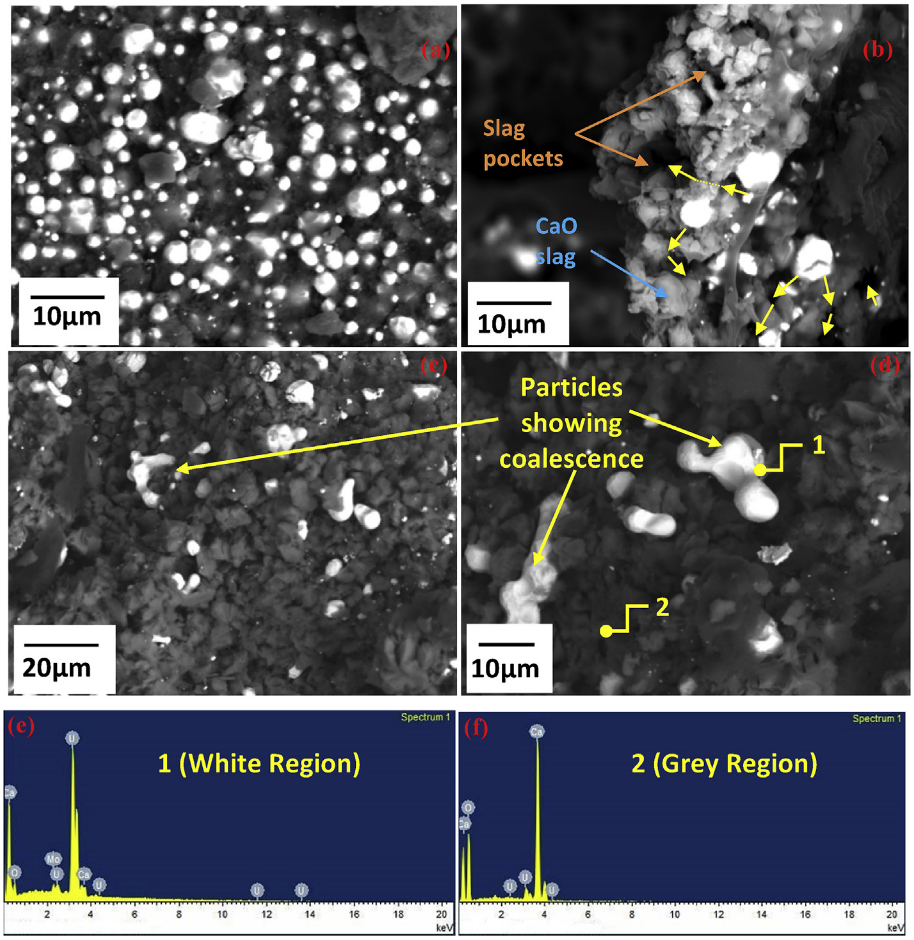

Fig. 6. SEM – BSE images of the reduced hard mass obtained after calciothermic reduction of UO_2 in the presence of Mo (Fig. 6(a) through 6(d)); Fig. 6(e) and (f) represent the typical EDS spectrums for the white and grey regions in the SEM images of the reduced hard mass.

Table 4
Effect of the process parameters on the characteristics of the final alloy powder in the R-D experiments.

Exp. Code	Process Parameters	Avg. Composition of the R-D powder (wt% Mo, from EDS data)	Standard Deviation (σ or SD)	Phases present in the alloy powder
RD-1	1150 °C, 4 h	23.21	25.57	α, γ, γ'
RD-2	1300 °C, 1 h	2.59	3.08	α, γ, γ'
RD-3	1300 °C, 4 h	10.58	1.59	γ
RD-4	1300 °C, 5 min	14.12	10.44	α, γ, γ'
RD-5	970 °C, 4 h	The reduced mass was not leached to obtain powder in this case.		

(Fig. 5(b)) confirms the presence of U predominantly at the periphery of the particle, whereas there is no uranium at all in the core of the particle. The elemental map for Mo (Fig. 5(c)) shows an intensified green colour in the core of the particle, and a green colour of lower intensity elsewhere. Thus, it is clear that the particle contains an unalloyed Mo core, surrounded by region containing both U and Mo. The concentration of U outside the core, as seen in the line scan, is nearly constant over the region between the core and the periphery. This is due to the fact that there is a continuous supply of liquid U from the surrounding pores or pockets in the slag to the region of lower U (higher Mo) concentration, as a result of chemical driving force arising due to difference in Mo (or U) concentration.

These observations indicate that U-Mo alloy formation occurs in steps, (i) enveloping of a Mo particle by liquid U, and (ii) outward dissolution or diffusion of Mo (solute) into U (solvent). Due to very less time available for homogenization, i.e. 5 min, it was possible to capture and analyze particles where incomplete alloying could be seen (Fig. 5 and Fig. 4(a)) and hence unalloyed Mo was present in the core surrounded by U-Mo alloy region. The alloying occurs via a shrinking core mechanism [42], which has also been used to explain the alloy formation in case of Sm_2Fe_{17} and Y-Ni alloys by R-D process [34,39].

As the alloying progresses, the Mo core will shrink in size due to dissolution of Mo in uranium. Hence, the topology of Mo particles is retained initially in the alloy particles as seen in Fig. 4(d), which vanishes with time, as the molten alloy when it is kept above the liquidus temperature (1252 °C) of the U–10 wt%Mo alloy for prolonged time, will grow into spherical particles to minimise the total surface energy. When it tries to grow against the constraints put by the slag matrix, depressions arise over the surface of the alloy particle, as seen in Fig. 4(c).

Based upon the inferences drawn so far, the single particle alloying mechanism was identified to be the outward diffusion or

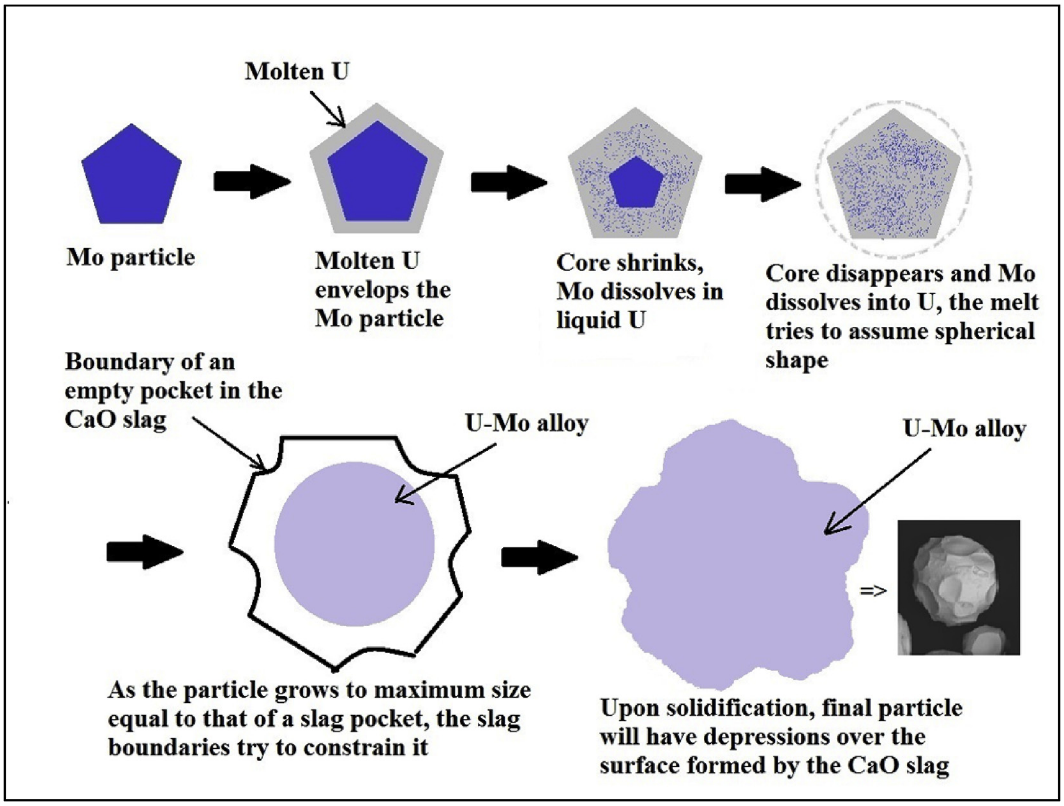

Fig. 7. Schematic showing the mechanism of alloying within a single particle.

dissolution of Mo into liquid U envelope surrounding the Mo particle. This mechanism is illustrated schematically in Fig. 7.

4.1.2. Particle-to-particle homogenization: the multi-particle system

To achieve particle-to-particle homogeneity, there should be exchange of one element or the other among the alloy particles, over time to attain equilibrium composition (close to 10 wt% Mo). The U particles are in general spherical or rounded and are dispersed in the calcium oxide slag as can be seen in Fig. 6(a) and (b). The CaO slag contains empty pockets or pores, of irregular geometry, which are interconnected. Hence, the liquid alloy can move from one pocket to other through these interconnected paths. Some particles which show signs of coalescence were also observed, as in Fig. 6(c) and (d). Such a morphology is possibly the result of liquid U alloy (containing Mo) flowing from one pocket to the other under the effect of chemical driving force, due to difference in Mo concentration existing between the slag pockets. As the soaking temperature was 970 °C which is much below the melting point of U, the local rise in temperature due to exothermic heat of the reduction reaction might have raised the temperature locally to keep the alloy (containing U and Mo) liquid in the regions seeing the high temperature, but the heat of the reaction would not be sufficient to maintain the charge at higher temperature for prolonged time. Hence, the liquid that had flown between the pockets solidified in situ and retained the shape of the pockets, as soon as its temperature fell below its melting point; thus giving rise to morphology as is seen in Fig. 6(d).

The movement of liquid alloy from one slag pocket to the other occurs under the effect of chemical driving force due to Mo concentration gradient existing in a direction opposite to movement of the liquid. This movement has two different aspects:

1) If a smaller pocket has lower Mo wt%, and a nearby bigger pocket has higher Mo wt%, the liquid U will move from smaller pocket to bigger pocket to equalize the concentration of the solute (Mo, to 10 wt%) → coarsening at such locations will occur, bigger particle will grow consuming the smaller one; thus giving rise to rounded interconnected particles with protrusions on the surface.
2) If a bigger pocket has lower Mo wt%, and a nearby smaller pocket has higher Mo wt%, the liquid U will move from bigger pocket to smaller one, thus shrinking in size and increasing the size of the smaller one; to equalize the concentration of the solute (Mo, to 10 wt%) → no coarsening will occur at such locations. Instead, the morphology will resemble that of two spheres connected by a pipe, which when repeated in three dimensions will give rise to skeleton-like structure even at higher soaking temperature. This proposition is supported by the fact that the skeleton-like structure observed in SEM of RD-1 (1150 °C, 4 h) shown in Fig. 8(a) is preserved even when soaking is done for 4 h at 1300 °C (Fig. 8(b)). However, at higher temperature (above the liquidus of the alloy), the individual particles in the skeleton are more connected and the skeleton has more developed arms as compared to that at lower temperature, because liquid has sufficient flowability so as to move from one pocket to another. Moreover, the skeleton-like structure seen in case of soaking for 4 h at 1150 °C is devoid of Mo, because that particular region did not see higher temperature for longer time to maintain U in liquid state, so the U could not move to envelope an adjacent Mo particle and solidified in-situ. In contrast, the skeleton-like structure at 1300 °C has a composition close to 10 wt% Mo, which explains the need to hold the charge at a temperature above the liquidus of the alloy for homogenization to occur.

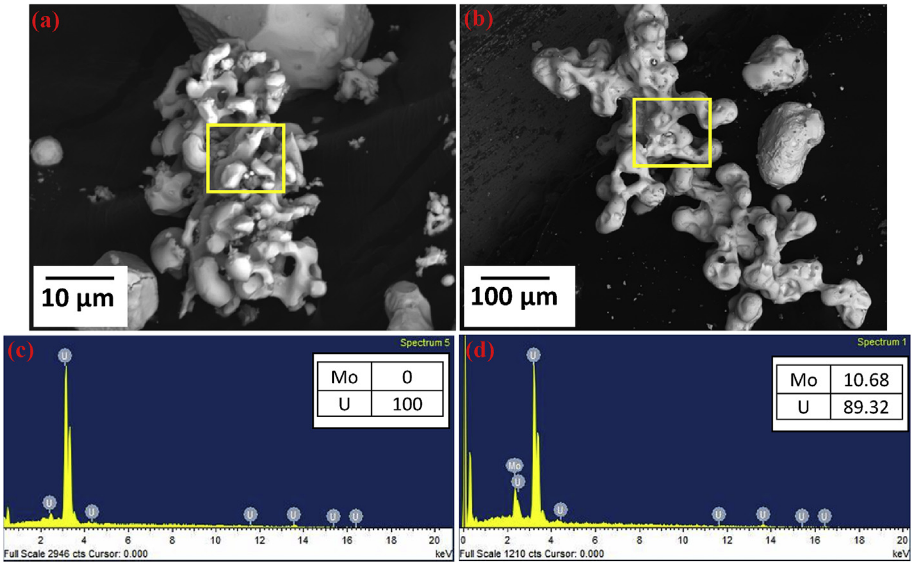

Fig. 8. SEM – BSE images of the skeleton-like structures observed under different soaking conditions (a) 1150 °C, 4 h (b) 1300 °C, 4 h; the corresponding EDS spectrums in Fig. 8(c) and (d) show the EDS data of the regions marked with boxes (yellow) in Fig. 8(a) and (b) respectively. (For interpretation of the references to colour in this figure legend, the reader is referred to the Web version of this article.)

The average concentration of Mo in the system will eventually approach the equilibrium one, i.e. 10 wt%, when sufficient soaking time is available above the liquidus temperature of the alloy, as is achieved with a soaking of 4 h at 1300 °C. The movement of liquid U, the final particle size and morphology and particle-to-particle homogeneity is decided by the following factors: (i) size of the slag pockets (ii) the concentration of Mo (solute) in the liquid (U) within each pocket (iii) soaking temperature and (iv) soaking time at higher soaking temperature. The mechanism governing the homogenization of Mo concentration throughout the system is

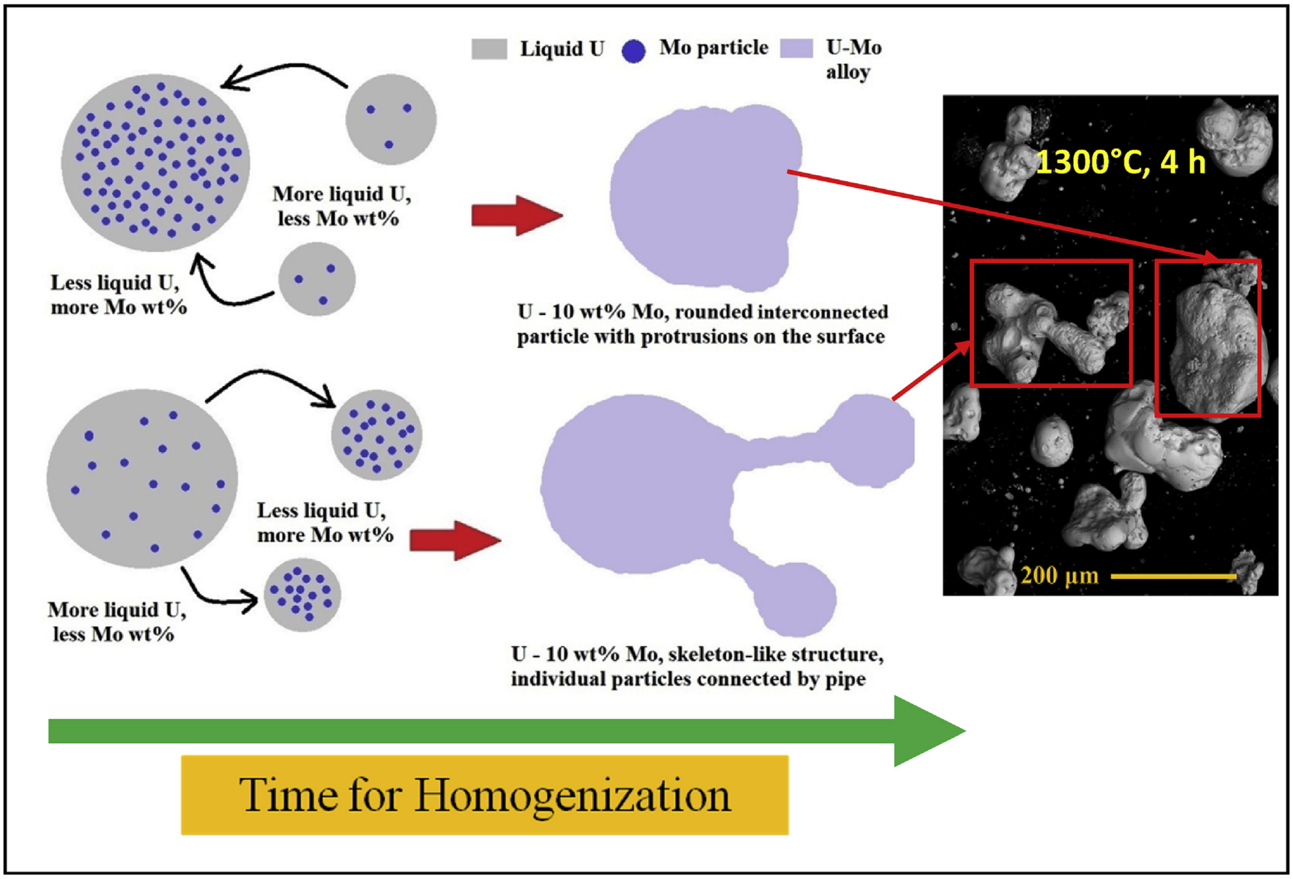

Fig. 9. Schematic showing the mechanism of particle-to-particle homogenization.

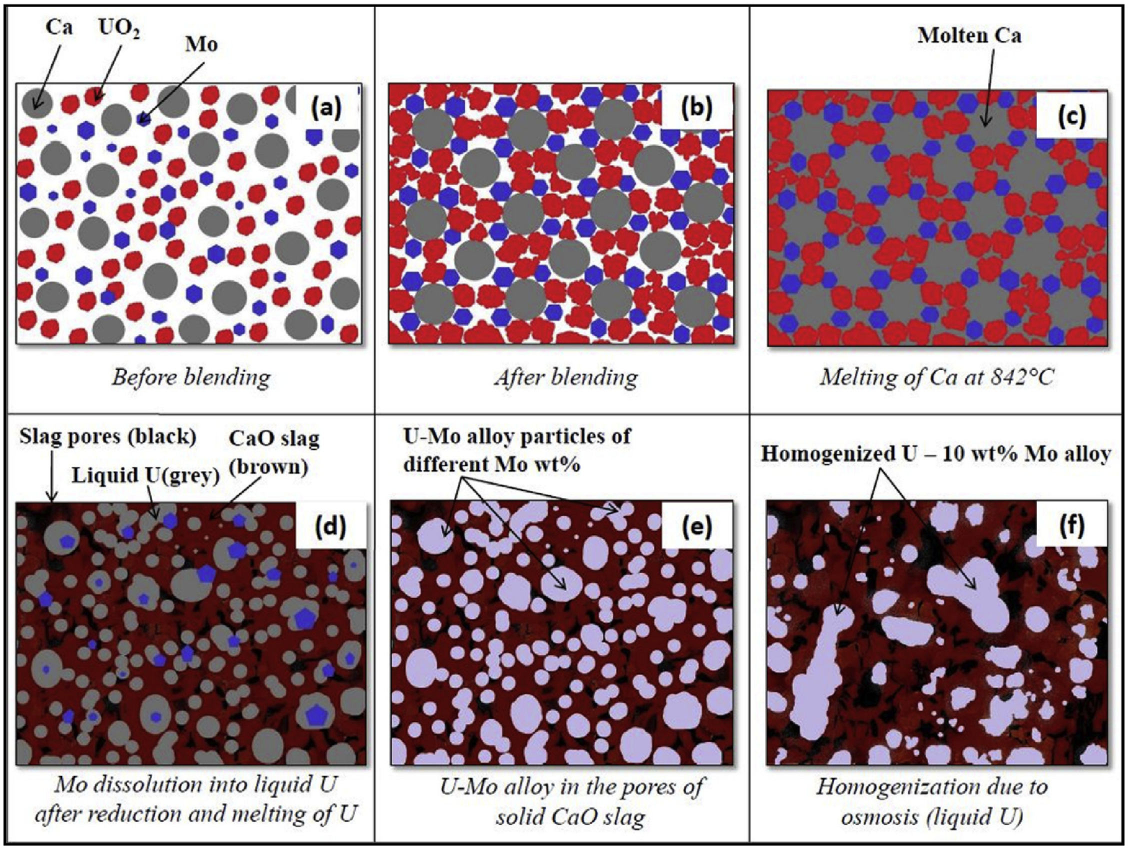

Fig. 10. Different Stages in the reduction – diffusion process: **(a)** The mixture at room temperature before blending **(b)** The mixture after blending; particles come closer together so that the only empty spaces are the voids between any two particles **(c)** Calcium melts at 842 °C filling the voids between the particles and covers the particles uniformly, facilitating reduction **(d)** After reduction and melting of U, molten metal droplets and solid Mo particles are entrapped in porous CaO slag which is solid; Mo dissolves in liquid uranium **(e)** U-Mo alloy liquid in the pores of the solid CaO slag **(f)** The liquid U at higher temperature moves from its higher concentration (lower Mo wt%) to its lower concentration (higher Mo wt%) under a chemical driving force, thus homogenization occurs with time such that every particle is U – 10 wt% Mo alloy.

illustrated by a schematic diagram in Fig. 9.

The different changes occurring in the state of the system as a function of time (t) and temperature (T) as depicted in Fig. 10 are

1) At T = Room Temperature, all the charge is solid. Blending is done to bring particles closer together, so that the only empty spaces left would be the voids between any two particles ($t = 0$, T = RT: Mechanical mixture before blending; $t = t_1$, T = RT: Blended mixture, Fig. 10(a)and (b))
2) At $t = t_2$ and T = 842 °C, calcium melts and surrounds/covers the particles intimately. The blended mixture of UO_2 and Mo is submerged in molten calcium. Reduction of UO_2 by Ca occurs and heat of the reduction reaction is sufficient to melt uranium; but may not be enough to sustain melting and also heat losses will be more for smaller size of the system; hence heating is continued above the melting point of U and soaking at higher temperature is given (Fig. 10(c))
3) At $t = t_3$, the system takes the form of a porous solid (high melting 2572 °C) CaO slag network with molten uranium present in the slag pockets or pores; Mo is distributed randomly among these slag pockets, submerged in the molten uranium. The liquid U envelops the Mo particle and alloying occurs due to dissolution of Mo into the liquid U (Fig. 10(d)and 10(e))
4) The liquid U moves from one pocket where concentration of liquid is more (solute Mo is less) to other pocket in the vicinity where concentration of liquid is less (solute Mo is more) under chemical driving force, so as to equalize U wt% and thus Mo wt% in each particle. Given soaking for sufficient time at higher temperature, the average concentration of Mo in the system will eventually approach the equilibrium one, i.e. 10 wt% (Fig. 10(f))

4.2. Gamma phase stability

The intent of this research work is to achieve fully stabilized gamma phase in the U-Mo alloy, which can be achieved under furnace cooling condition with a minimum of 8 wt% Mo, as explained earlier [4,19]. Hence, this was true for U-10 wt%Mo alloy prepared by R-D under the suitable soaking conditions. The XRD plot shown in Fig. 2 corroborates this fact.

The present work however involves in situ formation of U-Mo alloy powder after reduction of UO_2, where metal is melted locally (dispersed in non-melting CaO slag) and alloying is achieved by local diffusion of Mo into U. Therefore the local cooling rates are expected to be higher than that of conventional alloy making processes, even when the average cooling conditions are similar to furnace cooling condition. So, it was expected that even with 4 wt% Mo, gamma phase could be stabilized completely. However, the XRD plot for U-4wt%Mo alloy in Fig. 2 shows the presence of peaks corresponding to all the three phases, α, γ and γ'; which are the equilibrium phases at 4 wt% Mo as is evident from the U-Mo phase diagram shown in Fig. 11 [43]. This clearly explains that the cooling rates in case of R-D process are in no way greater than the cooling rates in furnace cooling conditions, which necessitates a Mo concentration greater than 8 wt% for complete stabilization of the isotropic γ phase.

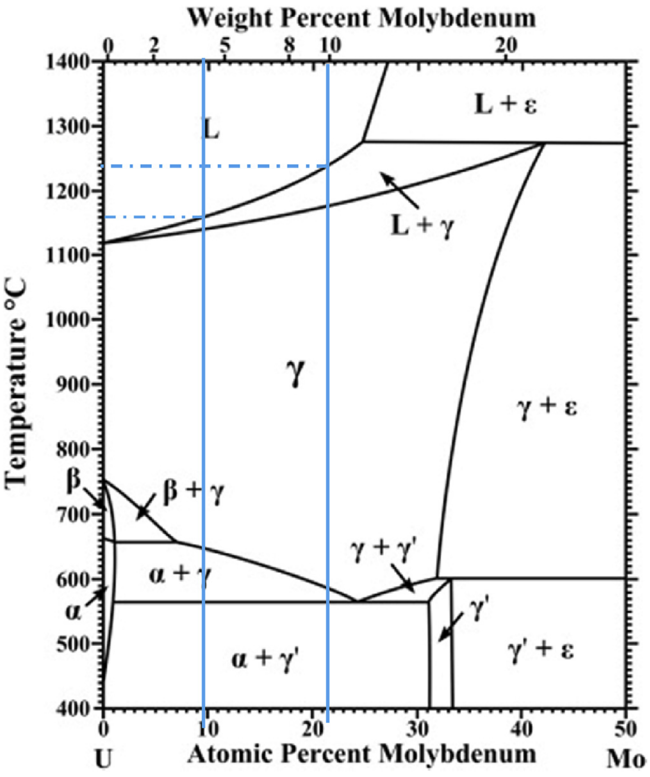

Fig. 11. The partial U-Mo phase diagram in the compositional range of interest [43].

5. Conclusions

U-10 wt%Mo alloy has been successfully prepared by R-D process and complete stabilization of desired isotropic γ-phase has been achieved at optimum process parameters of 1300 °C and 4 h. Understanding of the mechanism of the R-D process for the U-Mo system has also been achieved and the mechanism has been proposed based on experimental evidence. It has been identified that atomistic diffusion of U or Mo, through the porous slag, between two slag pockets, followed by inter-diffusion of U and Mo within a single particle, are two dominant mechanisms adopted by the system, for homogenization and reaching the equilibrium composition. The above two mechanisms are sped up if the temperature of the charge (i.e. reduced metal + Mo + slag) is kept sufficiently higher than the liquidus of the alloy of interest. The flow of liquid between two slag pockets and the inter-diffusivities of each species increase dramatically in the liquid state, due to its open structure. At soaking temperatures below the liquidus of the particular alloy, only solid state diffusion of Mo in U will be prevalent, which is itself sluggish in nature. This necessitates longer soaking periods to achieve homogeneous and equilibrium composition. In addition, the driving force for preferential solute movement ceases to exist due to absence of liquid U. Therefore, it was preferred to choose a soaking temperature above the liquidus temperature of the alloy, in order to achieve homogeneity and equilibrium in practical time spans.

Acknowledgements

The authors are grateful to Dr. Madangopal Krishnan, Associate Director, Materials Group for providing the opportunity to embark upon this research work and showing his keen interest in the work. The authors are thankful to Shri Pramendra Singh, Shri U.B. Naik and all other staff in our lab for their extended support while carrying out the calciothermic reduction and leaching experiments. The authors also thank Dr. Bhaskar Paul of MP&CED for his support in carrying out the DTA experiment. The authors also thank Shri K.N. Hareendhran and Shri S.V. Kadam of Quality Control Section, UED in carrying out the chemical analysis of the alloy powders.

Appendix A. Supplementary data

Supplementary data to this article can be found online at https://doi.org/10.1016/j.jallcom.2019.03.204.

References

[1] A. Travelli, The U.S. Reduced enrichment research and test reactor (RERTR) program, in: Proceedings of the 1978 International Meeting on Reduced Enrichment for Research and Test Reactors, ANL/RERTR/TM–1, Argonne, Illinois, November 9-10, 1978, pp. 3–18.

[2] S. Van den Berghe, P. Lemoine, Review of 15 years of high-density low-enriched UMo dispersion fuel development for research reactors in Europe, Nucl. Eng. Technol. 46 (2) (2014) 125–146. https://doi.org/10.5516/NET.07.2014.703.

[3] V.P. Sinha, P.V. Hegde, G.J. Prasad, G.K. Dey, H.S. Kamath, Phase transformation of metastable cubic gamma-phase in U-Mo alloys, J. Alloys Compd. 506 (1) (2010) 253–262. https://doi.org/10.1016/j.jallcom.2010.06.187.

[4] V.P. Sinha, P.V. Hegde, G.J. Prasad, G.K. Dey, H.S. Kamath, Effect of molybdenum addition on metastability of cubic γ-uranium, J. Alloys Compd. 491 (1) (2010) 753–760. https://doi.org/10.1016/j.jallcom.2009.11.060.

[5] S. Neogy, M.T. Saify, S.K. Jha, D. Srivastava, M.M. Hussain, G.K. Dey, R.P. Singh, Microstructural study of gamma phase stability in U-9wt.%Mo alloy, J. Nucl. Mater. 422 (1–3) (2012) 77–85. https://doi.org/10.1016/j.jnucmat.2011.12.005.

[6] J.L. Snelgrove, R.F. Domagala, G.L. Hofman, T.C. Wiencek, G.L. Copeland, R.W. Hobbs, R.L. Senn, The Use of U_3Si_2 Dispersed in Aluminum in Plate-type Fuel Elements for Research and Test Reactors, Argonne National Laboratory, 1987. ANL/RERTR/TM–11.

[7] V.P. Sinha, G.P. Mishra, S. Pal, K.B. Khan, P.V. Hegde, G.J. Prasad, Development of powder metallurgy technique for synthesis of U_3Si_2 dispersoid, J. Nucl. Mater. 383 (1–2) (2008) 196–200. https://doi.org/10.1016/j.jnucmat.2008.08.046.

[8] M. Ugajin, A. Itoh, M. Akabori, N. Ooka, Y. Nakakura, Irradiation behavior of high uranium-density alloys in the plate fuels, J. Nucl. Mater. 254 (1) (1998) 78–83. https://doi.org/10.1016/S0022-3115(97)00347-4.

[9] T.C. Wiencek, S.L. Hayes, G.L. Hofman, M.K. Meyer, Irradiation behavior of U_6Mn-Al dispersion fuel elements, J. Nucl. Mater. 278 (2–3) (2000) 358–363. https://doi.org/10.1016/S0022-3115(99)00280-9.

[10] R.F. Domagala, G.L. Copel, G.L. Hofman, Irradiation behavior of low-enriched U_6Fe-Al dispersion fuel elements, J. Nucl. Mater. 150 (2) (1987) 238–243.

[11] Development Status of Metallic, Dispersion and Non-oxide Advanced and Alternative Fuels for Power and Research Reactors, IAEA-TECDOC-1374, Vienna, 2003, p. 49.

[12] K.H. Kim, D.B. Lee, C.K. Kim, G.E. Hofman, K.W. Paik, Characterization of U-2 wt% Mo and U-10 wt% Mo alloy powders prepared by centrifugal atomization, J. Nucl. Mater. 245 (2–3) (1997) 179–184. https://doi.org/10.1016/S0022-3115(97)00011-1.

[13] A.N. Holden, Physical Metallurgy of Uranium, Addison-Wesley Publishing Co., Inc., USA, 1958.

[14] D.D. Keiser Jr., A.B. Robinson, J.-F. Jue, P. Medvedev, D.M. Wachs, M.R. Finlay, Microstructural development in irradiated U-7Mo/6061 Al alloy matrix dispersion fuel, J. Nucl. Mater. 393 (2) (2009) 311–320. https://doi.org/10.1016/j.jnucmat.2009.06.018.

[15] V.P. Sinha, G.J. Prasad, P.V. Hegde, R. Keswani, C.B. Basak, S. Pal, G.P. Mishra, Development, preparation and characterization of uranium molybdenum alloys for dispersion fuel application, J. Alloys Compd. 473 (1–2) (2009) 238–244. https://doi.org/10.1016/j.jallcom.2008.05.061.

[16] W.D. Wilkinson, in: Uranium Metallurgy, vol. 2, Interscience Publishers, 1962, pp. 855–1230. Uranium Corrosion and Alloys.

[17] A. Travelli, Status and Progress of the RERTR Program in the Year 2004, IAEA-CN–140, International Atomic Energy Agency (IAEA), 2004. https://inis.iaea.org/collection/NCLCollectionStore/_Public/36/069/36069517.pdf.

[18] K.H. Kim, D.B. Lee, C.K. Kim, I.H. Kuk, K.W. Baek, Development of Uranium-Silicide and U-Mo Alloy Fuels by Centrifugal Atomization, 1997. IAEA-TECDOC–970, https://inis.iaea.org/collection/NCLCollectionStore/_Public/29/000/29000279.pdf.

[19] K. Tangri, G.I. Williams, Metastable phases in the uranium molybdenum system and their origin, J. Nucl. Mater. 4 (2) (1961) 226–233. https://doi.org/10.106/0022-3115(61)90129-5.

[20] S. Neogy, M.T. Saify, S.K. Jha, D. Srivastava, G.K. Dey, Ageing characteristics of the metastable gamma phase in U–9 wt.% Mo alloy: experimental observations and thermodynamic validation, Phil. Mag. 95 (26) (2015) 2866–2884.

https://doi.org/10.1080/14786435.2015.1081300.

[21] J.M. Park, H.J. Ryu, K.H. Kim, D.B. Lee, Y.S. Lee, J.S. Lee, B.S. Seong, C.K. Kim, M. Cornen, Neutron diffraction analyses of U–(6–10 wt.%) Mo alloy powders fabricated by centrifugal atomization, J. Nucl. Mater. 397 (1–3) (2010) 27–30. https://doi.org/10.1016/j.jnucmat.2009.11.026.

[22] J. Lisboa, J. Marin, M. Barrera, A. Navarrete, L. Olivares, Atomization of U-Mo Particles under nitrogen atmosphere, World J. Nucl. Sci. Technol. 6 (2016) 43–52. https://doi.org/10.4236/wjnst.2016.61004.

[23] C.R. Clark, B.R. Muntifering, J.-F. Jue, Production and characterization of atomized U-Mo powder by the rotating electrode process, in: 2007 International Meeting on Reduced Enrichment for Research and Test Reactors (RERTR), INL/CON-07-13156, Idaho National Laboratory (INL), 2007. https://inldigitallibrary.inl.gov/sites/sti/sti/3874558.pdf.

[24] M.K. Meyer, C.R. Clark, Fuel powder production from ductile uranium alloys, in: 1998 International Meeting on Reduced Enrichment for Research and Test Reactors (RERTR), INIS-BR–3884, Sao Paulo, Brazil, October 18 - 23, 1998. https://www.rertr.anl.gov/Fuels98/CClark.pdf.

[25] J.P. Blackledge, G.G. Libowitz, in: W.M. Mueller (Ed.), Metal Hydrides, 1968.

[26] M. Durazzo, C.J. Rocha, F. Mestnik, M. Ricardo, N. Leal, Powder fabrication of U-Mo alloys for nuclear dispersion fuels, in: International Nuclear Atlantic Conference, INIS-BR–10680 Brazil, 2011 (2011).

[27] R. Cech, Rare earth intermetallic compounds by a calcium hydride reduction diffusion process, U.S. Patent 3,748,193, issued July 24, 1973.

[28] T.S. Krishnan, Preparation of rare earth-cobalt magnet alloy by reduction-diffusion process, Bull. Mater. Sci. 2 (3) (1980) 161–165.

[29] C.K. Gupta, Chemical Metallurgy, Wiley-VCH Verlag GmbH & Co. KGaA, Weinheim, 2003, pp. 383–384.

[30] G. Qi, M. Hino, A. Yazawa, Experimental study on the reduction-diffusion process to produce Fe–Nd, Fe–Sm, Co–Nd and Co–Sm alloys, Mater. Trans., JIM 31 (6) (1990) 463–470. https://doi.org/10.2320/matertrans1989.31.463.

[31] J. Lin, S. Liu, X. Qian, J. Bayi, M. Su, Synthesis of Nd_2Fe_{17} by reduction-diffusion process, J. Alloys Compd. 238 (1–2) (1996) 113–115. https://doi.org/10.1016/0925-8388(95)02130-2.

[32] Eneida da G. Guilherme, H.R. Hechenberg, José Octavio A. Pascoal, Reduction-diffusion preparation of $Nd_{15}Fe_{77}B_8$, $NdFe_{11}Ti$, $NdFe_{10.5}Mo_{1.5}$ and $NdFe_{10.75}Mo_{1.25}$ alloys for magnets, Mater. Sci. Forum 530 (2006) 181–186. Trans Tech Publications, https://doi.org/10.4028/www.scientific.net/MSF.530-531.181.

[33] D.L. Martin, Nickel-lanthanum alloy produced by a reduction-diffusion process, U.S. Patent 3,883,346, issued May 13, 1975r.

[34] G. Deng, Q. Jing, X. Wang, G. He, X. Ye, Synthesis mechanism of Sm_2Fe_{17} alloy produced in reduction-diffusion process, J. Rare Earths 28 (2010) 420–424. https://doi.org/10.1016/S1002-0721(10)60357-2.

[35] S. Okada, K. Suzuki, E. Node, K. Takagi, K. Ozaki, Y. Enokido, Preparation of submicron-sized $Sm_2Fe_{17}N_3$ fine powder with high coercivity by reduction-diffusion process, J. Alloys Compd. 695 (2017) 1617–1623. https://doi.org/10.1016/j.jallcom.2016.10.306.

[36] C.S. Teixeira, L. Caron, A. Anastasopol, S.W.H. Eijt, J.A. Lozano, E. Brück, P.A.P. Wendhausen, A new feature of the reduction–diffusion process applied for the synthesis of magnetocaloric $LaFe_{13-x}Si_x$ compounds, J. Alloys Compd. 541 (2012) 84–87. https://doi.org/10.1016/j.jallcom.2012.05.112.

[37] R.O. Suzuki, T. Ueki, M. Ikezawa, T.H. Okabe, T. Oishi, K. Ono, A fundamental study on preparation of Al_3Ti powders by calciothermic reduction of oxides, Mater. Trans., JIM 32 (3) (1991) 272–277. https://doi.org/10.2320/matertrans1989.32.272.

[38] R.O. Suzuki, K. Tatemoto, H. Kitagawa, Direct synthesis of the hydrogen storage V–Ti alloy powder from the oxides by calcium co-reduction, J. Alloys Compd. 385 (1–2) (2004) 173–180. https://doi.org/10.1016/j.jallcom.2004.04.137.

[39] M. Ilayaraja, L.J. Berchmans, S.R. Sankaranarayanan, Synthesis of Y-Ni alloy by calciothermic reduction diffusion process, Metall. Mater. Eng. 21 (2) (2015) 65–72. https://doi.org/10.30544/96.

[40] A.S.M. Handbook, Powder metal technologies and applications, ASM Int. 7 (1998) 89–91.

[41] J.-M. Oh, W. Kim, B.-K. Lee, C.-Y. Suh, H.-S. Kim, J.-W. Lim, New method for preparation of low oxygen Mo powder by reduction of MoO_3 using Ca, Powder Metall. 57 (4) (2014) 291–294. https://doi.org/10.1179/1743290113Y.0000000083.

[42] Octave Levenspiel, Chemical Reaction Engineering, John Wiley & Sons, Inc., 1999, pp. 569–580.

[43] M.A. Steiner, E. Garlea, S.R. Agnew, Modeling solute segregation during the solidification of γ-phase U-Mo alloys, J. Nucl. Mater. 474 (2016) 105–112. https://doi.org/10.1016/j.jnucmat.2016.02.035.